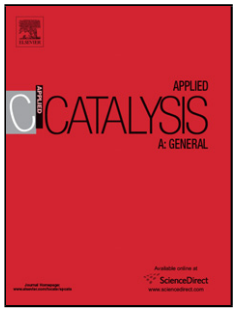

Title: Preparation of Ni-Mo_2C/Carbon Catalysts and their Stability in the HDS of Dibenzothiophene

Authors: Haiyan Wang, Shida Liu, Rubenthran Govindarajan, Kevin J. Smith

PII: S0926-860X(17)30164-3
DOI: http://dx.doi.org/doi:10.1016/j.apcata.2017.04.008
Reference: APCATA 16206

To appear in: *Applied Catalysis A: General*

Received date: 6-2-2017
Revised date: 31-3-2017
Accepted date: 14-4-2017

Please cite this article as: Haiyan Wang, Shida Liu, Rubenthran Govindarajan, Kevin J.Smith, Preparation of Ni-Mo2C/Carbon Catalysts and their Stability in the HDS of Dibenzothiophene, Applied Catalysis A, Generalhttp://dx.doi.org/10.1016/j.apcata.2017.04.008

Preparation of Ni-Mo_2C/Carbon Catalysts and their Stability in the HDS of Dibenzothiophene

Haiyan Wang, Shida Liu, Rubenthran Govindarajan, Kevin J. Smith*

Department of Chemical and Biological Engineering, University of British Columbia, 2360 East Mall, Vancouver, B.C., V6T 1Z3, Canada.

*Corresponding author. Tel.: +1 6048223601; Fax: +1 6048226003.

E-mail address: kjs@mail.ubc.ca (K. J. Smith)

Graphical Abstract:

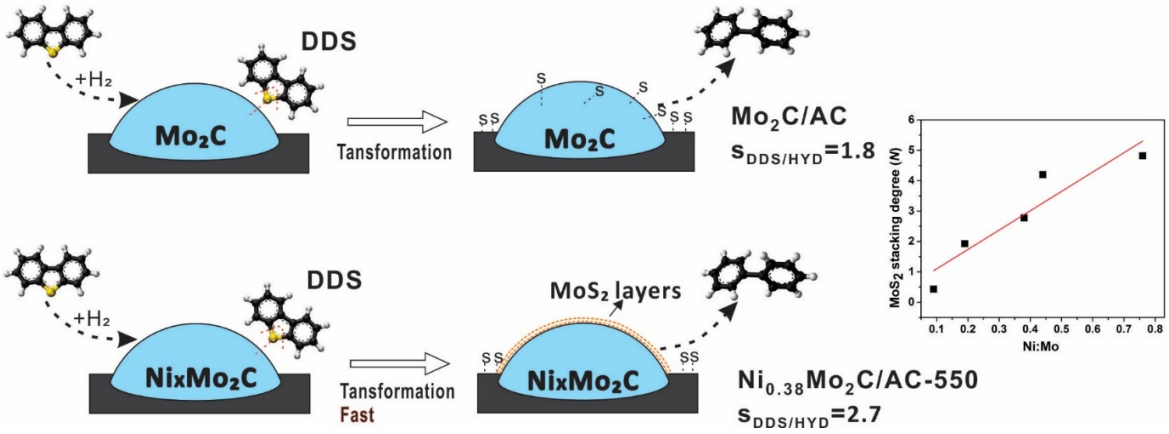

Highlights:

- Carbothermal hydrogen reduction (CHR) temperature decreased to 550 °C by Ni addition in Ni-Mo_2C/carbon catalyst synthesis.
- Ni addition increases S uptake during HDS, resulting in the rapid formation of Mo_2C-MoS_2 core-shell structures.
- The core-shell Mo_2C-MoS_2 structures promote direct desulfurization (DDS) of dibenzothiophene.
- HDS activity of Mo_2C enhanced with Ni addition up to Ni:Mo < 0.38.

Abstract

The HDS activity and stability of Ni-Mo_2C/AC catalysts, prepared by carbothermal hydrogen reduction (CHR) at different temperatures and with different Ni:Mo ratios, is reported. The highest HDS activity occurred for catalysts with Ni:Mo ratios of 0.38 and 0.19, when prepared at the relatively low CHR temperature of 550 and 600 °C, respectively. Partial sulfidation of the Ni-Mo_2C/AC catalysts occurred rapidly upon reaction in 2 wt% dibenzothiophene (DBT) at 350 °C and 2.1 MPa H_2. Uptake of S was enhanced with increased Ni content, resulting in the formation of Mo_2C-MoS_2 core-shell structures. The stack height of

the MoS_2 shell increased with increased Ni content and promoted the direct desulfurization of DBT.

Keywords: Molybdenum carbide; Promoter; Hydrodesulfurization (HDS); Carbothermal hydrogen reduction; Dibenzothiophene

Introduction

Hydrodesulfurization (HDS) [1] is an important processing step in heavy oil upgrading that uses $NiMoS/Al_2O_3$ or $CoMoS/Al_2O_3$ catalysts to facilitate S removal from heteroaromatic compounds present in the heavy oil [2, 3]. Novel catalysts, such as metal carbides and nitrides, have also been investigated as potential hydrotreating catalysts over the past several decades [4-6], in part because of their noble metal-like catalytic properties [7-10]. Sajkowski and Oyama [11] reported that a Mo_2C/Al_2O_3 catalyst had twice the HDS activity of a conventional MoS_2 catalyst when measured at 633 K and 13.0 MPa H_2 using a gas oil with 116 ppm S. The comparison was made based on the number of active sites as measured by CO uptake. Similarly, Da Coasta et al. [12] reported that a Mo_2C/Al_2O_3 catalyst doped with P was more active than an industrial hydrotreating catalyst for aromatics hydrogenation, HDS and hydrodenitrogenation

(HDN) when measured at industrial conditions (613 K, 3 MPa) using a gasoil with 47 ppm S content.

One of the difficulties encountered when applying Mo_2C catalysts for HDS is that they are unstable because of surface sulfidation, even in the presence of low concentrations of S (< 0.1 wt%). Aegerter et al. [13] proposed that a thin layer of highly dispersed MoS_2 is formed on the surface of Mo_2C or Mo_2N particles during thiophene HDS, as evidenced by IR and TPD-CO characterization of the catalysts. The authors proposed that Mo_2C and Mo_2N particles serve as rigid substrates for a sulfided Mo phase, exposing a large number of co-ordinatively unsaturated (cus) Mo sites, which results in increased activity of the catalyst (by 50%), compared to a conventional MoS_2 catalyst. Da Costa et al. [14] also reported that a Mo_2C catalyst became more active than a Co-Mo/Al_2O_3 commercial catalyst for the HDS of 4,6-dimethyldibenzothiophene (4,6-DMDBT) with low levels of S in the feed (<135 ppm). Oyama et al. [15] suggested the formation of a Mo-carbosulfide active site to explain product selectivities observed during the simultaneous conversion of sulfur, oxygen and aromatic compounds over Mo_2C, compared to the product selectivities measured with a single reactant, especially for the case of cumene hydrogenation. In another study, Brito and coworkers [16] presulfided a NiMo carbide catalyst prior to HDS and claimed that a Ni-Mo-S phase was responsible for the measured HDS activity. Guangzhou et al. [17] reported on NiMo carbide and Mo_2C catalyst performance for the HDS of dibenzothiophene (DBT) and pointed out that Ni addition increased the Mo_2C activity by 57 %,

although there was no conclusion drawn regarding the effect of S on the metal carbides during HDS. The transformation of Mo_2C catalysts in the presence of S-compounds remains somewhat unclear and the application of these catalysts for HDS in high S concentrations (as is the case for gas oils derived from residue oils, for example) has not been reported.

Several methods have been developed to synthesize Mo_2C catalysts, either as bulk, unsupported catalysts or as Mo_2C dispersed on high surface area Al_2O_3 [13] and carbon supports [18, 19]. The most common synthesis method uses temperature-programmed reduction (TPR) of metal oxides in mixtures of H_2 and a hydrocarbon such as CH_4 [20] or C_2H_6 [21]. However, the resulting low surface area and carbon residue on the catalyst surface means that the catalysts have relatively low activity. An alternative preparation method uses carbothermal hydrogen reduction (CHR), employing a carbon support and pure H_2 to generate the metal carbide at high reduction temperatures (700-800 ^oC). This method yields nanoparticles of Mo_2C, as first demonstrated by Mordenti et al. [22] and Liang et al. [23] and also reported previously by the authors [24]. Thus, CHR is a relatively facile method to synthesize carbon supported Mo_2C catalysts, in which the carbon support may also suppress coke formation during residue oil upgrading [25]. However, CHR has a limited capacity to achieve complete reduction/carburization of the catalyst precursor, even at high reduction temperatures. For example, in previous work [24], CHR of ammonium heptamolybdate impregnated activated charcoal (AC) yielded a mixed Mo_2C/MoO_xC_y phase with a relatively high portion of Mo_2C

(~50%) obtained at 700 ºC. However, almost half of the carbon support was hydrogenated (mostly to CH_4) during the CHR process, which decreased the support area available to achieve high dispersion of the Mo_2C.

One potential option to increase the Mo_2C dispersion is to add a second metal to decrease the synthesis temperature required for the formation of the metal carbide. Liang et al. [26] reported that the presence of Co decreased the CHR temperature for Mo_2C formation to 600 ºC, at a Co/Mo molar ratio of 1.0. They concluded that the Co increased the formation of CH_x species during CHR, facilitating carburization of the Mo. Similar effects have been reported in the synthesis of W_2C by CHR using Ni as the promoter [27, 28]. The presence of the 2nd metal has also been shown to provide synergistic effects in the case of Co added to Mo_2C when used for the chemo-selective reduction of nitroarenes, with the Co-Mo_2C/AC catalyst having significantly higher activity than the Mo_2C/AC alone [29]. Moreover, the bimetallic carbides formed in the presence of Mo and other transition metals [30, 31] such as Fe, Co and Ni, show effective catalytic activity in hydrotreating reactions.

The present study reports on the CHR synthesis of Ni-Mo_2C supported on activated carbon (AC) and their application to the HDS of DBT at high S concentrations (~ 3500 ppm) that mimic the S content of heavy oil [1]. New data are reported that capture the effect of Ni content on the formation of the Ni-Mo_2C catalysts and their resulting HDS catalytic activity. In particular, the

changes in catalyst morphology that occur during reaction, with the formation of a core-shell MoS_2-Mo_2C structure, is reported for the first time. The structural changes are related to the stability of the Ni-Mo_2C/AC and the Mo_2C/AC catalysts.

2. Experimental

2.1 Catalyst Preparation

Activated charcoal (AC: 1025 m^2/g, pore volume 0.85 mL/g) was impregnated with a solution of ammonium heptamolybdate (AHM) in acetone (10 %) and H_2O (90 %) and rotary evaporated under vacuum to remove all the solution. The resulting solid was aged in air for 4 h before drying at 110 ^oC overnight to yield the precursor. The precursor was then calcined in N_2 at 300 ^oC for 5 h to obtain the oxide states of Mo, Ni or bimetallic NiMo. The calcined precursor (ca. 1.8 g) was placed in a U-tube reactor and subsequently converted to the Ni-Mo_2C/AC catalyst by CHR in a continuous H_2 flow (200 mL (STP)/min), while increasing temperature from room temperature to 500 ^oC at 10 ^oC /min, followed by increasing temperature at 1 ^oC/min to 650 ^oC and holding the final temperature for 90 min before quenching to room temperature in N_2 [24]. This catalyst (designated as 10%Mo_2C/AC-650) was compared with Ni-Mo_2C/AC catalysts, prepared similarly but with successive impregnations of the AC with solutions of AHM and $Ni(NO_3)_2$, respectively, to obtain precursors with different Ni:Mo ratios. After calcination, the precursors were converted to Ni-Mo_2C/AC by CHR as described above but with final

reduction temperatures of 550 ºC or 600 ºC. The resulting Ni-Mo_2C catalysts with different Ni:Mo ratio (from 0.02-0.76) are designated as Ni_xMo_2C-y, where x represents the Ni:Mo atomic ratio and y represents the reduction temperature (ºC). The 10% Mo_2C/AC-650 and Ni-Mo_2C/AC catalysts, used in the batch reactor to determine reaction kinetics, were loaded into the batch reactor without passivation. The catalysts were transferred from the preparation U-tube reactor to the batch reactor in a glove bag under a N_2 blanket to ensure minimal air exposure. For the catalyst stability tests conducted in the trickle-bed reactor and for the characterization of the fresh catalysts (XRD, BET), the catalyst samples were first passivated in a flow of 1 vol % O_2/N_2 at room temperature for 2 h prior to the analysis and a mild pre-reduction of the passivated catalysts was done prior to the reaction test. Carbon supported MoS_2 (MoS_2/AC) was also used herein as a reference to compare with the used Ni-Mo_2C/AC catalysts. The MoS_2/AC precursor was prepared similarly to the Mo_2C/AC precursor followed by ex-situ presulfiding in a 100 mL decalin for 3 h at 350 ºC under approximately 10 vol%H_2S/H_2 generated from CS_2 (with further details provided in the Supporting Information).

2.2 Catalyst Characterization

Elemental analysis of the catalysts was conducted by inductively coupled plasma atomic emission spectroscopy (ICP-OES). All samples were acid digested in aqua regia at 110 ºC to extract all metals from the support, prior to the analysis. The adsorbed S on the used catalysts

was determined using a Perkin-Elmer 2400 series II CHNS/O Analyzer. The combustion temperature was set at 975 ^{o}C.

The Brunnauer-Emmett-Teller (BET) surface area, pore volume and pore size of the calcined Ni-Mo_2C precursors, passivated Ni-Mo_2C and used catalysts (following HDS reaction) were determined from N_2 adsorption/desorption isotherms measured at -196 ^{o}C using a Micromeritics ASAP 2020 analyzer. The used catalysts were washed with acetone several times before analysis to remove the decalin solvent used in the reaction. About 0.1 g of the sample was degassed at 200 ^{o}C (100 µm Hg) for 4 h prior to the measurement. The BET surface area was calculated from the adsorption isotherm in the relative pressure range (P/P_o) of 0.1-0.6. The total pore volume (V_{total}) was obtained based on the total N_2 adsorption measured at P/P_o= 0.99. The micropore volume (V_{micro}) was obtained by the t-plot method using data measured in the range of P/P_o = 0.18-0.50. The mesopore volume was calculated from the desorption isotherm and the average pore diameter was calculated assuming a cylindrical pore such that $d_{pore}= 4V_{total}/S_{BET}$.

A Bruker D8 Focus (0-20, LynxEye detector) diffractometer was used to identify the bulk phases of the synthesized passivated catalysts using a Co Kα (λ=1.789 Å) radiation source. The instrument was operated at 35 kV and 40 mA in a scan range of 2Θ = 5-90 ^{o} with a step size of 0.04 ^{o} and scan speed of 0.5 s/step. After background subtraction, phase identification was

processed using standard software. The XRD of the fresh and used catalysts were compared to identify bulk phase changes of the catalysts during reaction.

X-ray photoelectron spectroscopy (XPS) analysis was conducted using a Leybold Max200 spectrometer for surface analysis of the used catalysts. Mg Kα was used as the photon source generated at 1253.6 eV. For a survey scan, the pass energy was set at 192 eV; for a narrow scan, it was set at 48 eV. The C 1s peak was taken as the reference peak at 284.5 eV to account for charging effects. Exposure of the samples to the atmosphere prior to analysis was minimized to less than 2 minutes.

Transmission electron microscope (TEM) images of the supported catalysts were generated using a (JEOL) JEM 2200FS electron microscope operated at 200 kV, with a 1.9 Å point-to-point resolution. Used catalysts were analyzed to identify the particle size distribution and characteristic slabs of the synthesized/formed species. The samples were prepared by dispersion in ethanol and then sonicated for several minutes. A drop of the suspension was placed on a 230 mesh copper grid coated with Formvar-Carbon film and then dried in a vacuum chamber. The clusters/particles identified in the TEM images were measured and counted to yield a size distribution that was fitted to a lognormal distribution to determine the average size of the cluster/particle. The number of formed MoS_2 layers was also counted based on the TEM images

and the stacking degree (N) of MoS_2 was calculated as $N = \sum_{i=1..t} n_i N_i / \sum_{i=1..t} n_i$, where n_i is the number of stacks with N_i layers.

A time of flight secondary ion mass spectrometer (TOF-SIMS; a PHI TRIFT V instrument) was used in the static SIMS mode to analyse the used catalysts and to identify changes in catalyst surface properties (with or without Ni as a promoter) following the HDS reaction. TOF-SIMS yields both elemental and molecular ions, and hence it can provide detailed information on the upper layer of the used catalysts. The catalyst samples were sputtered by a primary ion beam of Au^+ before the spectra were collected, both in the positive and negative mode. For each analysis the delivered ion dose was 6.3×10^{11} ion/cm^2, and the total sputtering time for each spectrum was approximately 1800 s. The detected mass range was within 0-1850 amu and triplicate spectra were collected at three different points across the prepared samples with a raster size of 400.0 µm × 400.0 µm as representative sample areas.

2.3 Catalytic Tests for Hydrodesulfurization

The HDS of dibenzothiophene (DBT) was carried out in a 300 mL stirred-batch reactor (Autoclave Engineers) to assess the catalytic activities of the as-prepared Ni-Mo_2C/AC fresh catalysts with different Ni:Mo ratios (Ni:Mo = 0 ~ 0.76). The experiments were operated at 350 ^oC with an initial H_2 pressure of 2.1 MPa with ca. 2.0 wt% of DBT (0.35 wt% S) as the reactant in 100 mL decalin. Dissolution of DBT in decalin was assisted by sonication, which also

removed dissolved air from the prepared liquid feed. The catalyst was added to obtain 0.13-0.14 g_{metal}/100 mL liquid in the slurry. The fresh catalyst and O-free reactant liquid were placed in the reactor sequentially, under a N_2 blanket using a glove bag. The reactor was then sealed and flushed with N_2 to remove residual air from the reactor. After a leak test, ultra-high purity H_2 was used to first flush and then fill and pressurize the reactor to the desired level, following which the reactor was heated to a pre-determined temperature within 35 mins. After the reaction period (up to 5 h) the reactor was cooled to room temperature and de-pressurized. Liquid samples were recovered periodically during the reaction and analyzed using a Shimadzu (QP-2010-S) GC/MS and RTX5 30 m × 0.25 mm capillary column based on an internal calibration method. The internal standard used in this study was diphenylmethane (DPM). Overall, the activity data reported herein were measured with a carbon balance $\geqslant$ 94% and several experiments were repeated to quantify the error in the activity data.

A trickle bed reactor (length 50 cm, hot zone 30 cm with an internal diameter of 8.64 mm) operated in a down-flow mode was also used to compare the stability of the $Ni_{0.19}Mo_2C$/AC-600 and 10 % Mo_2C/AC-650 catalysts. The experiments were operated at 310 ^oC at a constant pressure of 4.1 MPa. The liquid feed, consisting of ca. 2.0 wt% DBT in decalin, was fed to the reactor by means of a high-pressure piston pump (Gilson model 307). The H_2 flow was controlled by a mass flow controller (Brooks 5850TR). All the experiments were operated with a H_2/feed volumetric ratio of 600 and a liquid-hourly space velocity (LHSV) of 8 h^{-1}. The liquid

product was collected periodically from a condenser placed after the reactor exit and held at room temperature. Finally, all samples were analyzed using gas chromatography (Shimadzu GC) by a capillary column (SHRXI-5MS, 15 m x 0.25 mm x 0.25 um) and a FID detector. Before performing the activity test, the passivated catalyst (ca. 0.77 g, 2.5 mL) was activated in-situ under H_2 flow at 400 ^oC for 2 h to remove the passivation layer from the catalyst surface.

3. Results

3.1 Catalyst Characterization

3.1.1 XRD Analysis

XRD analysis of the calcined Ni-Mo_2C/AC catalyst precursors showed an amorphous structure, indicating a high dispersion of metals on the support (Figure S1, Supplementary Information). Figure 1 presents the XRD patterns of the Ni-Mo_2C/AC catalysts with Ni:Mo ratios of 0-0.76, and prepared at different CHR temperatures (Figure 1(a): 550 ^oC; Figure 2(b): 600 ^oC). Included at the top of both Figure 1 (a) and (b) are the spectra for 10%Mo_2C/AC-750, the unpromoted Mo_2C prepared at a reduction temperature of 750 ^oC to show the positions of β-Mo_2C (PDF card # 00-036-0787). Mo_2C is detected in all the diffractograms of Figure 1, with diffraction peaks at 2θ = 40.12°, 44.21°, 46.14°, 61.35°, 72.87°, 82.97°, 86.58° and 89.51° and no other bulk phases of MoO_x present in the samples. At a reduction temperature of 550 ^oC, the peak intensities of Mo_2C increased with increased Ni:Mo ratio in the range of 0.02-0.44 and the

same phenomenon occurred at a reduction temperature of 600 ºC, but for a narrower Ni:Mo ratio of 0.02 to 0.19. Figure 1(b) shows that when Ni:Mo ratio is > 0.19, the intensities of the Mo_2C reflections do not increase, however other phases are detected. The peaks at 51.28 º and 60.23 º are assigned to metallic Ni (PDF card # 00-004-0850) and the separation of Ni from the Mo_2C can be observed when the Ni:Mo ratio is > 0.38 at both reduction temperatures of 550 ºC and 600 ºC. A clear phase separation of Ni from the Mo_2C was also reported by Puello-Polo et al. [31] and Santillán et al. [30] when synthesizing the catalysts using the same metal salts as those used herein. The Ni-Mo bimetallic carbide ($Ni_6Mo_6C_2$, PDF card # 01-089-4883) was detected with diffraction angles 2θ = 47.76º, 50.51º and 53.40º when the Ni:Mo ratio reached 0.38 at both reduction temperatures, whereas nickel carbide was not detected in any of the samples.

Analysis of the XRD data for the Ni_xMo_2C/AC-600 catalysts ($0 \leqslant x \leqslant 0.19$) yields a small decrease in the Mo_2C lattice parameters with increased Ni content (Table 1). The diffraction angles also shifted to higher diffraction angles for the $Ni_{0.19}Mo_2C$/AC-600 compared to the unmodified catalyst (10%Mo_2C/AC750), implying some incorporation of Ni into the β-Mo_2C crystal structure. Thus, the interaction between Ni and Mo_2C occurs at low Ni loadings. The lattice parameters at higher Ni contents were not determined because of Ni phase separation and the crystallite sizes are not calculated from the XRD data because small particles of Mo_2C are air sensitive and re-oxidize during analysis.

3.1.2 Catalyst Composition and BET Analysis

The measured Ni:Mo ratios of the catalysts are reported in Table 2. The carbon loss (burn off%) from the AC support that occurred during CHR (Table 2) increased with increased Ni:Mo ratio and increased reduction temperature. During CHR, the AC support reacts with the H_2, mostly forming CH_4, as determined by GC-FID analysis of the product gases (Figure 2). The maximum concentration of CH_4 in the product gas from the CHR was ~2.0 mol% at 650 ^oC for the unpromoted Mo_2C (Figure 2 (a)), whereas, in the presence of Ni, the CH_4 concentration was significantly higher (up to ~ 6 mol%), even at 600 ^oC. Figure 2(b) shows that the maximum in the CH_4 content of the CHR product gas increased with increased Ni content. Furthermore, the CH_4 formation profiles are different between the unpromoted and Ni- promoted Mo_2C. In the former case, the CH_4 content doubles every 50 ^oC in the temperature interval 550 ^oC~650 ^oC and remains approximately constant during the hold period; whereas, for the Ni-Mo_2C precursors, the CH_4 concentration decreases significantly above the highest reduction temperature of 600 ^oC. The burn-off mass (carbon loss) for the unprompted Mo_2C reduced at 650 ^oC was ~ 18 wt%, similar to the $Ni_{0.19}Mo_2C$/AC-550 (reduced at 550 °C), clearly indicating that the presence of Ni accelerates the carbon loss at low temperature, which reduces the carburization time required for the Mo precursor. Also note that the burn-off mass is well correlated with CH_4 formation during CHR (Figure S2, Supporting Information).

After CHR, the shape of the N_2 adsorption isotherms were similar to the AC support (Figure S3, Supporting Information). The surface area of the catalysts prepared at a CHR temperature of 550 ^oC did not show a significant change with increased Ni content; whereas, at 600 ^oC, the surface area decreased with increased Ni content (Table 3 and Figure S4, Supporting Information). Moreover, both catalysts showed a general trend of increased pore size with increased Ni content and the increase was due to an increase in mesopore volume (Figure S4).

3.2 Catalyst Characterization after Reaction

All the catalysts were characterized after the HDS reaction to identify potential changes in the catalyst chemical and physical properties. In addition, the MoS_2/AC catalyst properties are reported here as a comparator for the used Ni-Mo_2C/AC catalyst properties. The catalysts were separated by high speed centrifuge from the slurry recovered from the batch reactor. The solid fraction was then washed in acetone and dried overnight under a N_2 blanket in a glove bag. Prior to XPS and TEM analysis, the dried samples were degassed in vacuum at 200 ^oC for 4 h. The transfer of the samples to the vacuum chamber (XPS, TEM) was done within 5 min to minimize exposure to air.

3.2.1 XRD and BET Analysis

XRD analysis of the used catalysts (Figure S5, Supporting Information) showed no change in the Mo_2C bulk structure after reaction, indicating that the Mo_2C crystallites are resistant to

bulk sulfidation under the chosen reaction conditions, consistent with the observation made by Aegerter et al. [13]. There were no peaks that could be assigned to S compounds in the XRD pattern of the used catalysts either.

The BET analysis data (Table 3) generally indicate that after the HDS reaction, there was a significant loss in catalyst surface area, whereas the average pore size and mesopore volume fraction increased, implying that mostly micropores were blocked during reaction.

3.2.2 XPS and CHNS Analysis

The effect of increased Ni:Mo ratio on the XPS spectra of the used catalysts is shown in Table 4 and Figure 3. The elemental surface compositions clearly show the presence of S on the catalyst surface after the HDS of DBT, consistent with data reported by Sajkowski and Oyama [11]. As illustrated in Table 4, the used Ni-Mo_2C catalysts reduced at 550 ^oC have higher S content than the same catalysts reduced at 600 ^oC. In addition, the Ni-Mo_2C catalysts all have higher S content after reaction than the Mo_2C catalyst with no Ni addition.

Apart from a clear increase in S content on the catalyst surface with increased Ni addition, the Mo 3d XPS spectra of Figure 3 (a) and (c) show an obvious shift from lower B.E. to higher B.E. as Ni content increases, indicative of the formation of Mo-S surface species. The Mo 3d shift to higher B.E. on the Ni-Mo_2C is greater than that of the Mo_2C/AC, indicating more sulfidation of the Mo in the presence of the Ni.

Figure 4 compares the Mo 3d and S 2p XPS spectra of the $Ni_{0.19}Mo_2C$/AC-550 catalyst after reaction for different periods to that of the MoS_2/AC catalyst. The S 2p peak at B.E.= 162.2 eV confirms the presence of Mo-S surface species, consistent with the results from the Mo 3d spectra. In addition, it is noted that the Mo 3d B.E. of the Ni-Mo_2C catalyst surface is relatively stable after 1 h of reaction and clearly different from that of the MoS_2/AC surface. Table 5 also shows that the S species accumulate during reaction since the S content (i.e. the atomic ratio of S to Mo or S wt%) increased with increased reaction time for all catalysts. The S content (wt%) measured by CHNS and reported in the last column of Table 5, does not show a clear difference between the two catalysts. However, the S wt% calculated based on the XPS data give clear differences between these two catalysts, showing a strong ability of S adsorption in the presence of Ni. For the 10%Mo_2C/AC-650 catalyst, the S:Mo ratio increased from 0.30 to 0.59, whereas for the Ni-Mo_2C it is increased from 0.69 to 0.99, indicating a faster sulfidation of the Ni-Mo_2C catalyst.

3.2.3 TOF-SIMS Analysis

The negative ion mass spectrum of Mo, sulfur or oxysulfide (oxide) spectra were recorded during sputtering from a catalyst sample area of 400 × 400 μm. Several interesting Mo characteristic fragments containing oxygen, sulfur or both were detected in the used catalysts, such as MoS^- or MoO_2 (m/z=130), $MoOS^-$ or MoO_3 (m/z=146), MoO_2S^- or MoS_2 (m/z=162), MoO_3S^- (m/z=178) and MoO_2S_2 (m/z=194). The presence of sulfur indicates that the surface of

the catalyst has been changed during the HDS reaction with the formation of Mo-O-S or Mo-S bonds on the catalyst surface. In order to eliminate possible variations between samples, the normalized ion intensity yield (i.e. relative intensity, RI) is used to make comparisons. The distribution of identified Mo oxysulfide species (MoO_xS_y) is represented by the abundance of each Mo oxysulfide species divided by the abundance of all MoO_xS_y ions (RI'). The identified molecular fragments and their relative abundance are reported in Table 6. These data confirm the adsorption of S on the catalyst surface during reaction and indicate that in the presence of Ni, the amount of MoS surface species is almost 2x's higher than that on the unpromoted Mo_2C (Ni:Mo=0), consistent with the XPS analysis results.

3.2.4 TEM Analysis

The TEM micrographs of the used Ni-Mo_2C/AC catalysts reduced at 600 ^oC with various Ni:Mo ratios are presented in Figure 5 and 6. The formation of core-shell like structures is clearly visible, suggesting that a Mo_2C core is surrounded by MoS_2 generated during the HDS reaction. The size of the core-shell structure increases from 9.7 nm to 20.2 nm as Ni content increases, as shown by the lognormal distribution data of Figure 5. The Mo_2C-MoS_2 clusters become agglomerated when the Ni:Mo ratio > 0.44. At low Ni content, such as $Ni_{0.02}Mo_2C$/AC-600, the contrast between particle and support is low and it is difficult to quantify the particle size from the TEM micrograph. For the 10%Mo_2C/AC-650, the characteristic slabs of MoS_2 are

difficult to identify as shown in Figure S6. Note also that the number of MoS_2 layers formed around the Mo_2C core increases with increased Ni content, as reported in Figure 6.

3.3 Catalyst Performance in HDS of DBT

Dibenzothiophene (DBT) was chosen as the model reactant to determine the activity of the prepared catalysts. The results of the activity tests at 350 ^oC for Ni-Mo_2C/AC catalysts, prepared at different reduction temperatures and Ni:Mo ratios are presented in terms of DBT conversion in Table S1 (Supporting Information). The mass of catalyst used for each activity measurement varied to account for the AC mass loss during the various CHR conditions, however, the total Mo+Ni mass remained relatively constant (~0.14 g_{metal}/100 mL_{feed}) for all experiments. The data of Table S1 (Supporting Information) show that the DBT conversion on Ni-Mo_2C/AC reduced at 550 ^oC was generally higher than the DBT conversion measured on the unpromoted Mo_2C/AC catalyst and higher than the DBT conversion measured on the Ni-Mo_2C/AC reduced at 600 ^oC, provided the Ni:Mo ratio is $<$ 0.44. The data clearly show improved activity of the Mo_2C in the presence of Ni. The conversion over the Ni-Mo_2C/AC-550 catalyst increased with increased Ni content for Ni:Mo ratios of 0-0.38, but decreased when the ratio increased above 0.38. The decreased conversion is likely due to the Ni phase separation that occurs at high Ni content and higher carbon loss (burn-off%) above a Ni:Mo ratio of =0.38 that may also decrease Mo dispersion. Similar observations with respect to increased HDS activity of P-doped Ni-

Mo_2C/Al_2O_3 catalysts with increased Ni content, were reported by Sundaramurthy et al. [32], using gas oils derived from Athabasca bitumen.

Kinetic analysis of the batch reactor data is complicated by the fact that the Mo_2C-based catalysts undergo sulfidation during reaction and consequently, their activity and selectivity may change with reaction time in the batch reactor. As shown in Table 5, the S content of the catalysts (with or without Ni addition) increases with reaction time. However, the difference in the amount of sulfur adsorbed on the 10%Mo_2C/AC-650 and $Ni_{0.19}Mo_2C$/AC-600 is constant at ~0.27 At% independent of reaction time (Table 5, column 3). This indicates that Ni has the ability to increase S adsorption but the effect of the Ni occurs rapidly within the 1st hour of reaction. The continued adsorption of S beyond this period is a consequence of the carbon support. Furthermore, Figure 4 shows that there is no visible difference with respect to the Mo oxidation state of the catalyst after the 1st hour of the reaction. To confirm the stabilization of the catalysts, Figure 7 reports the DBT conversion as a function of time-on-stream for the Mo_2C and the $Ni_{0.19}Mo_2C$/AC-600 catalysts measured at 310 ^oC and 4.1 MPa H_2 pressure and a LHSV of 8 h^{-1} in the downflow, fixed-bed reactor. A rapid decrease in DBT conversion occurs within the first 60 mins of operation beyond which both the DBT conversion and product selectivities stabilize. Continued operation beyond 5000 min showed that the activity of the $Ni_{0.19}Mo_2C$/AC-600 catalyst remained stable, whereas the DBT conversion over the Mo_2C/AC showed a small decline. Hence, to minimize these catalyst stabilization effects on the kinetic analysis of the

batch reactor data, only data collected after 1 h operation are included in the analysis. Hence, the kinetic analysis is performed on the partly sulfided, but stabilized Mo_2C-based catalysts.

The kinetics of the HDS of DBT on all the synthesized catalysts were determined assuming 1st-order reactions and a reaction pathway illustrated in Figure S7 (Supporting Information) [33]. Direct desulfurization of DBT (the DDS pathway) to form biphenyl (BPh) competes with a hydrogenation pathway (the HYD pathway) in which DBT is converted to1,2,3,4-tetrahydrodibenzothiphene (THDBT) before S-removal to yield cyclohexylbenzene (CHB). The kinetic parameters of this simplified reaction scheme were estimated using a Levenberg-Marquardt nonlinear regression methodology to solve the relevant ODEs (Equations 1-4) as below.

$$\frac{dC_{DBT}}{dt} = -k_1 C_{DBT} - k_2 C_{DBT} \quad (1)$$

$$\frac{dC_{THDBT}}{dt} = k_1 C_{DBT} - k_3 C_{THDBT} \quad (2)$$

$$\frac{dC_{BPh}}{dt} = k_2 C_{DBT} \quad (3)$$

$$\frac{dC_{CHB}}{dt} = k_3 C_{THDBT} \quad (4)$$

The 1st-order estimated kinetic rate constants k_j, $j=1\text{-}3$, are reported in Table 7 and the model fit to the data is shown in Figure S8 and Figure S9, for the CHR reduction temperatures of 550 °C and 600 °C, respectively, based only on the data obtained after a reaction time > 1 h. The

magnitude of the rate constant for the total consumption of DBT ($k_{total}=k_1+k_2$) (Table 7) indicates that the $Ni_{0.38}Mo_2C$/AC-550 and $Ni_{0.19}Mo_2C$/AC-600 have the highest activity among all the catalysts. Figure 8 shows that the rate constants k_1 and k_2 increase with increased Ni addition up to a maximum value and then decrease at high Ni contents. The thermal reactions are neglected since the thermal related conversions are very low (less than 5%).

The catalyst selectivity to the three main products of BPh, THDBT and CHB is illustrated in Figure S10. Biphenyl was the main product resulting from direct hydrogenolysis of the C-S bond of DBT, accounting for >80% of all products of the Mo_2C/AC-650 catalyst, and even higher for the Ni promoted catalysts, as shown from Figure S10 (a) and (d). These data imply that the DDS reaction route is dominant and is the preferred route for S removal on these Mo_2C-based catalysts. The data of Table 7, comparing the relative rates of DDS to HYD and reflected in the value of $S_{DDS/HYD}=k_2/k_1$, also suggests an increase in DDS selectivity with increased Ni/Mo ratio. The hydrogenated product CHB is mainly formed from the hydrogenation of THDBT and the data show that the presence of Ni increases CHB selectivity (Figure S10 (b), (c), (d) and (e)).

4. Discussion

The addition of Ni is shown to decrease the CHR temperature required for Mo_2C formation from the AHM/AC calcined precursor and this observation is in agreement with that reported previously by Liang et al. [26]. In a previous study [24] the optimized reduction temperature for

Mo_2C formation from AHM supported on AC was reported to be 650 ºC, whereas in the present study, we demonstrate that Mo_2C formation is possible at significantly lower CHR temperature (550 ºC) with Ni addition. Furthermore, the amount of Ni is shown to be critical in terms of the phases generated by CHR and in terms of the catalyst DBT activity. At a reduction temperature of 550 ºC, the formation of Mo_2C was confirmed by XRD when the Ni:Mo ratio is low (0.09). Since Ni activates H_2 at relatively low temperature [34, 35], hydrogenation of the carbon to yield CH_4 can occur at low temperature. In addition, by activating H_2 at relatively low temperature, Mo oxide is more readily reduced which makes the subsequent conversion to Mo carbide or oxycarbide more facile. As shown in Figure 2, the CH_4 concentration generated in the product gas from CHR of the $Ni_{0.19}Mo_2C$/AC-600 catalyst is ~4x's higher than that of the 10%Mo_2C/AC-650 catalyst when the reduction temperature reaches 600 ºC. In general, the concentration of CH_4 generated during CHR increases as the reduction temperature increases and as Ni loading increases. The XRD data show that as the amount of Ni increases, the intensity of the Mo_2C diffraction peaks increases. Figure 2 shows that the CH_4 generation rate increases rapidly above about 600 °C and Ni can lower this temperature. Hence, although temperature is the most important factor determining the CH_4 concentration measured during CHR, the Ni:Mo ratio also plays an important role in the reduction. We conclude that although the presence of Ni decreases the required reduction temperature for carbide formation, temperature remains the key factor in the CHR synthesis of metal carbides. However, higher temperature results in a higher degree of

crystallization and higher carbon loss (burn-off) from the carbon support. The burn-off was 48% for the $Ni_{0.76}Mo_2C$/AC-600 whereas at 550 ºC, the burn-off decreased significantly to only 28%. If we compare different Ni:Mo ratios, the difference in mass loss between Ni:Mo ratios of 0.02 and 0.19 is much larger than the mass loss between 0.19 and 0.76, suggesting that the effectiveness of Ni in increasing the CH_4 concentration is reduced at high Ni concentrations. When the Ni:Mo ratio reaches 0.38 at both 550 ºC and 600 ºC, $Ni_6Mo_6C_2$ species appear in the XRD, indicating that Ni has been incorporated into the Mo_2C structure during the CHR process. When the Ni:Mo ratio is > 0.38, metallic Ni appears. Unlike Mo_2C, the formation of $Ni_6Mo_6C_2$ and Ni are mostly dependent on Ni content rather than CHR temperature. Thus, the formation of the bimetallic carbide and Ni phase separation appears at the same Ni:Mo ratio despite differences in CHR temperature. Table 3 and Figure S4 show that when the catalyst precursors were reduced at 550 ºC, the surface areas were approximately constant at ~ 800 m^2/g for different Ni:Mo ratios; whereas, at a CHR temperature of 600 ºC, there was a clear decrease in surface area with increased Ni content. The differences are due to the fact that the pore widening process that occurs during CHR, removes some pore walls between mircopores causing a loss in surface area at 600 ºC; whereas, at 550 ºC the widening occurs, but since the pores are still developing, the pore walls and the resulting surface area remain intact. In addition, the catalyst pore size increased in the presence of Ni at both CHR temperatures, with most of the micropores

of the AC support enlarged into mesopores, which is beneficial for molecular diffusion of large molecules such as DBT.

XRD analysis of the fresh and used catalysts showed that the bulk phase properties of the catalysts were unchanged after reaction with DBT. However, CHNS and XPS analysis both showed that S was present on the surface of the used catalysts. Note that the measured d-spacing from the TEM is ~0.63 nm (Figure 6), indicating the formation of MoS_2 species on the used Ni-Mo_2C/AC catalysts [36]. A similar observation was reported by Zhang et al. [37] on a used Ni_2Mo_3N catalyst after hydrogenation in the presence of 100 ppm of thiophene. As shown in Table 4 and Figure S11, the amount of S increased with increased Ni content of the catalyst, suggesting that the Ni enhanced S adsorption on the metal sites. In addition, the TEM results confirmed this conclusion showing an increase in the number of MoS_2 layers with increased Ni content of the catalyst (Figure 6). Also note that the catalysts reduced at 550 ^oC had higher S content after use than those reduced at 600 ^oC. These results are consistent with the data obtained by CHNS analysis in which S content of the used catalysts is well correlated with the Ni:Mo ratio. The difference in S content of the catalyst as measured by CHNS (bulk analysis) versus XPS (surface analysis; reported in the last two columns of Table 4) can be accounted for by the S adsorbed inside the pores of the carbon support, the carbon “sink effect” proposed by Laine et al. [38]. There is a ~ 1.0 wt% difference between the bulk and surface S content of the Ni-Mo_2C catalysts reduced at 550 ^oC; whereas, the difference is ~ 0.5 wt% for the Ni-Mo_2C catalysts

reduced at 600 ºC. This difference is caused by the pore structure modification during CHR at different reduction temperatures. Since many micropores are destroyed at higher reduction temperature (600 ºC), the S adsorption capacity is decreased compared to the catalyst prepared at the lower CHR temperature.

XRD showed that Ni incorporates with Mo species during the CHR process. The calculated lattice parameters of β-Mo_2C decrease with increased Ni content before phase separation at high Ni content, which implies that smaller Ni atoms randomly substitute for Mo atoms in the metal carbide crystal structure. A similar conclusion was made by Wan and Leonard [39] in regards to Fe modified Mo_2C. XPS shows that the addition of Ni increased the S adsorption on to the catalyst surface after reaction with DBT. TEM analysis of the used Ni-Mo_2C/AC-600 catalysts (Figure 5) clearly showed that the Mo_2C particle size increased with Ni content. The catalyst metal carbide particle size is well correlated with Ni:Mo ratio as shown in Figure 9. Comparing the 10%Mo_2C/AC-650 and $Ni_{0.38}Mo_2C$/AC-600 catalysts with the same burn off shows an increase in particle size from 5 nm for the 10%Mo_2C/AC-650 catalyst to 15 nm for the $Ni_{0.38}Mo_2C$/AC-600 catalyst. Similar results were reported by Yao et al. [40] in their study of a NiMoC catalyst and Leonard and Wan [39] noted that unlike Fe, which decreases the size of Mo_2C particles, Ni will increase the size of Mo_2C. Figure 6 also shows that addition of Ni increases the number of MoS_2 layers in the MoS_2 shell that surrounds the Mo_2C of the used catalyst. Ni increases the stack number of MoS_2 as has also been reported on NiMoS/Al_2O_3

catalysts by Lercher et al. [35]. The STEM mode selected area analysis of the used catalyst shown in Figure 10, confirms that the Ni, Mo and S are closely bound in the used catalyst, suggesting that Ni can enhance the S interaction with Mo.

The present study has shown that Ni addition has a significant impact on both the CHR process and the S adsorption by the catalyst during the HDS reaction, and that both depend on the Ni content of the catalyst. During reaction, Ni enhances the adsorption of S by the Mo to form Ni-Mo-S on the outside of the Mo_2C particle, leading to the generation of a core-shell like structure. None of the characterization data, including the TOF-SIMS analysis, identified the presence of Mo carbo-sulfide structures, as proposed by Oyama et al. [15], and although they were not present as bulk species, we cannot exclude the possibility that they exist on the catalyst surface under reaction conditions.

The data of Table 7 and Figure S8 show that Ni added to the Mo_2C catalyst increases DBT conversion. A trend notable from Table 7 and Figure 8 is that k_2, representing catalytic ability to perform DDS, increases to a maximum value with increased Ni content. When the Ni concentration is relatively low, the added Ni is incorporated with Mo species into the final metal carbide phase. Thus, in the HDS of DBT, increased Ni increases the Mo_2S stacking number and according to the 'rim-edge' model of Chianelli and Daage [41], a higher stacking number yields higher DDS selectivity. However, when the Ni concentration is above a critical value (Ni:Mo >

0.38), the added Ni is not incorporated into the Ni-Mo carbide phase; on the contrary, more Ni causes phase separation and enlarges the particle size leading to less active sites and eventually lower activity. Also, available surface area is decreased by increased burn-off with increased Ni content, resulting in decreased dispersion of active sites and reduced activity. Moreover, more reduced single phase Ni contributes to the hydrogenation ability of the catalyst and thus, a decrease in $S_{DDS/HYD}$ is observed. Note that the trend of $S_{DDS/HYD}$ versus Ni content at 600 ^{o}C is not very clear, due to the loss of surface area along with Ni addition affecting the catalytic performance. For the above reasons, it is found that the best performing catalysts are $Ni_{0.38}Mo_2C$-550 and $Ni_{0.19}Mo_2C$-600. They have a total kinetic constant for DBT conversion of 1.11 and 1.14 mL/g_{metal}.min along with a very high $S_{DDS/HYD}$ ratio of 2.7 and 3.1, respectively.

5. Conclusions

Ni addition significantly reduces the temperature required for Mo_2C generation by CHR, with the presence of Mo_2C confirmed by XRD at a CHR temperature of 550 ^{o}C for a catalyst with a Ni:Mo ratio of 0.09. This CHR temperature is about 100 ^{o}C lower than that required to form Mo_2C in the absence of Ni. XRD and XPS show that Ni is incorporated into the Mo_2C structure during the CHR process and TEM showed that increased Ni content increased the Mo_2C particle size. However, for Ni:Mo > 0.38 phase separation occurred, decreasing the catalyst activity and the direct desulfurization selectivity. The Ni also increased the rate of S

adsorption leading to the formation of Mo_2C-MoS_2 core-shell structures. Increasing Ni content also increased the stack height of the MoS_2 shells, leading to a higher DDS selectivity in the HDS of DBT. The best performing catalysts in the HDS of DBT at 350 °C are $Ni_{0.38}Mo_2C$/AC-550, with a total kinetic constant of 1.11 mL/g_{metal}.min and $S_{DDS/HYD}$ of 2.7, and $Ni_{0.19}Mo_2C$/AC-600 with a total kinetic constant of 1.14 mL /g_{metal}.min and $S_{DDS/HYD}$ around 3.1.

Acknowledgements:

The financial support of the Natural Sciences and Engineering Research Council of Canada (NSERC) and Shell Canada is gratefully acknowledged. The authors would like to thank Dr. Ken Wong and Dr. John Kim from the Interfacial Analysis and Reactivity Laboratory at the University of British Columbia for XPS and TOF-SIMS measurements, respectively. Also, we would like to thank Dr. Xin Zhang from 4D Labs at Simon Fraser University for STEM measurements.

References:

[1] J.G. Speight, The desulfurization of heavy oils and residua, CRC Press, 1999.

[2] S. Badoga, R.V. Sharma, A.K. Dalai, J. Adjaye, Applied Catalysis A: General 489 (2015) 86-97

[3] Y. Sun, H. Wang, R. Prins, Catalysis Today 150 (2010) 213-217

[4] Y. Chen, S. Choi, L.T. Thompson, Journal of Catalysis 343 (2016) 147-156.

[5] J.-S. Choi, A.H. Zacher, H. Wang, M.V. Olarte, B.L. Armstrong, H.M. Meyer Iii, I.I. Soykal, V. Schwartz, Energy & Fuels 30 (2016) 5016-5026.

[6] E. Furimsky, Applied Catalysis A: General 240 (2003) 1-28

[7] D.R. Stellwagen, J.H. Bitter, Green Chemistry 17 (2015) 582-593.

[8] A. Szymańska, M. Lewandowski, C. Sayag, G. Djéga-Mariadassou, Journal of Catalysis 218 (2003) 24-31

[9] P.A. Aegerter, W.W.C. Quigley, G.J. Simpson, D.D. Ziegler, J.W. Logan, K.R. McCrea, S. Glazier, M.E. Bussell, Journal of Catalysis 164 (1996) 109-121.

[10] Y. Villasana, Y. Escalante, J.E.R. Nuñez, F.J. Méndez, S. Ramírez, M.Á. Luis-Luis, E. Cañizales, J. Ancheyta, J.L. Brito, Catalysis Today 220 (2014) 318-326

[11] D.J. Sajkowski, S.T. Oyama, Applied Catalysis A: General 134 (1996) 339-349.

[12] P. Da Costa, J.-M. Manoli, C. Potvin, G. Djéga-Mariadassou, Catalysis today 107 (2005) 520-530

[13] P.A. Aegerter, W.W.C. Quigley, G.J. Simpson, D.D. Ziegler, J.W. Logan, K.R. McCrea, S. Glazier, M.E. Bussell, Journal of Catalysis 164 (1996) 109-121

[14] P.D. Costa, C. Potvin, J.-M. Manoli, B. Genin, G. Djéga-Mariadassou, Fuel 83 (2004) 1717-1726.

[15] B. Dhandapani, T.S. Clair, S.T. Oyama, Applied Catalysis A: General 168 (1998) 219-228

[16] E. Puello-Polo, M. Ayala-G, J.L. Brito, Catalysis Communications 53 (2014) 9-14

[17] G. Jin, J. Zhu, X. Fan, G. Sun, J. Gao, Chinese Journal of Catalysis 27 (2006) 899-903.

[18] S.A.W. Hollak, R.W. Gosselink, D.S. van Es, J.H. Bitter, ACS Catalysis 3 (2013) 2837-2844

[19] A.L. Jongerius, R.W. Gosselink, J. Dijkstra, J.H. Bitter, P.C.A. Bruijnincx, B.M. Weckhuysen, ChemCatChem 5 (2013) 2964-2972.

[20] J.S. Lee, S.T. Oyama, M. Boudart, Journal of Catalysis 106 (1987) 125-133

[21] A. Hanif, T. Xiao, A.P.E. York, J. Sloan, M.L.H. Green, Chemistry of materials 14 (2002) 1009-1015

[22] D. Mordenti, D. Brodzki, G. Djéga-Mariadassou, Journal of solid state chemistry 141 (1998) 114-120

[23] C. Liang, P. Ying, C. Li, Chemistry of materials 14 (2002) 3148-3151

[24] H. Wang, S. Liu, K.J. Smith, Energy & Fuels 30 (2016) 6039-6049.

[25] M. Kouzu, Y. Kuriki, K. Uchida, K. Sakanishi, Y. Sugimoto, I. Saito, D. Fujii, K. Hirano, Energy & fuels 19 (2005) 725-730

[26] C. Liang, W. Ma, Z. Feng, C. Li, Carbon 41 (2003) 1833-1839.

[27] C. Liang, F. Tian, Z. Li, Z. Feng, Z. Wei, C. Li, Chemistry of materials 15 (2003) 4846-4853

[28] N. Ji, T. Zhang, M. Zheng, A. Wang, H. Wang, X. Wang, J.G. Chen, Angewandte Chemie 120 (2008) 8638-8641

[29] Z. Zhao, H. Yang, Y. Li, X. Guo, Green chemistry 16 (2014) 1274-1281.

[30] L.A. Santillán-Vallejo, J.A. Melo-Banda, A.I.R. de la Torre, G. Sandoval-Robles, J.M. Domínguez, A. Montesinos-Castellanos, J.A. de los Reyes-Heredia, Catalysis today 109 (2005) 33-41.

[31] E. Puello-Polo, J.L. Brito, Journal of Molecular Catalysis A: Chemical 281 (2008) 85-92.

[32] V. Sundaramurthy, A.K. Dalai, J. Adjaye, Applied Catalysis B: Environmental 68 (2006) 38-48.

[33] G.H. Singhal, R.L. Espino, J.E. Sobel, G.A. Huff, Journal of Catalysis 67 (1981) 457-468

[34] A.A. Smirnov, S.A. Khromova, D.Y. Ermakov, O.A. Bulavchenko, A.A. Saraev, P.V. Aleksandrov, V.V. Kaichev, V.A. Yakovlev, Applied Catalysis A: General 514 (2016) 224-234.

[35] E. Schachtl, E. Kondratieva, O.Y. Gutierrez, J.A. Lercher, The journal of physical chemistry letters 6 (2015) 2929-2932.

[36] P.A. Nikulshin, D.I. Ishutenko, A.A. Mozhaev, K.I. Maslakov, A.A. Pimerzin, Journal of Catalysis 312 (2014) 152-169.

[37] L. Zhang, J. Feng, Q. Chu, W. Li, K. Xu, T.S. Wiltowski, Catalysis Communications 66 (2015) 50-54.

[38] J. Laine, M. Labady, F. Severino, S. Yunes, Journal of Catalysis 166 (1997) 384-387

[39] C. Wan, B.M. Leonard, Chemistry of Materials 27 (2015) 4281-4288

[40] Z. Yao, J. Jiang, Y. Zhao, F. Luan, J. Zhu, Y. Shi, H. Gao, H. Wang, RSC Advances 6 (2016) 19944-19951.

[41] M. Daage, R. Chianelli, Journal of Catalysis 149 (1994) 414-427.

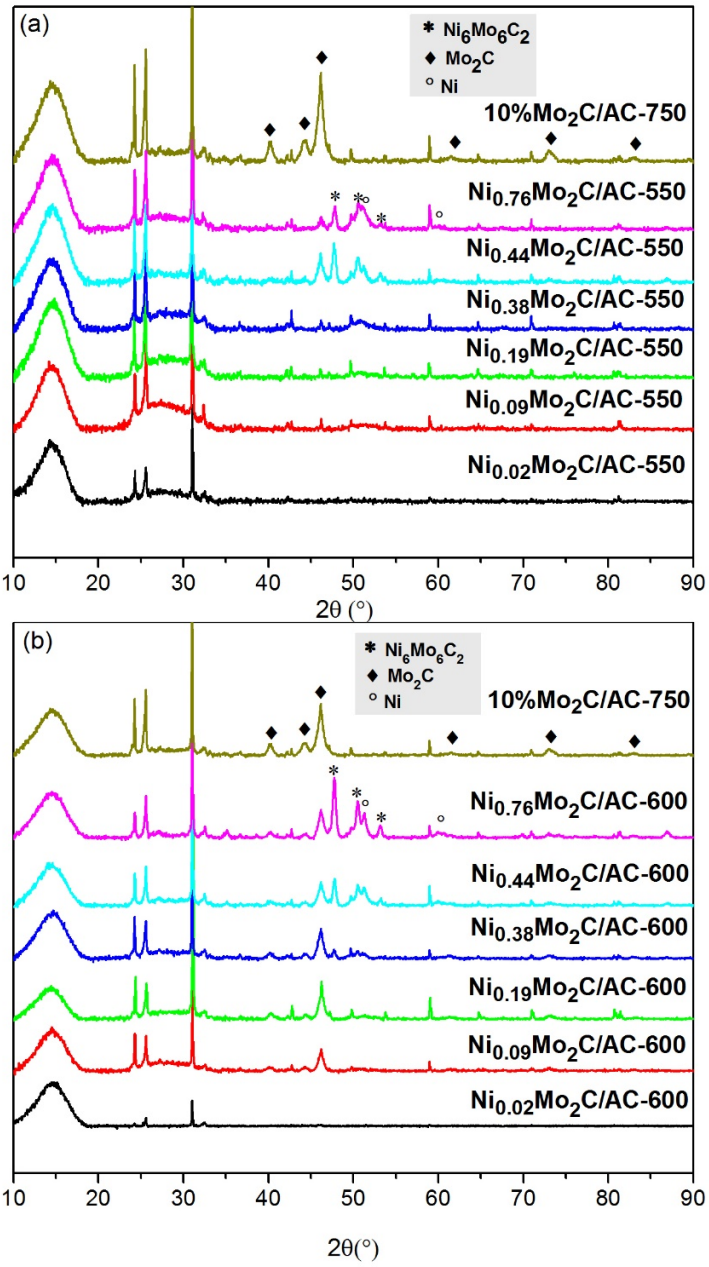

Figure 1: XRD patterns of Ni-Mo_2C/AC catalysts with different ratios of Ni:Mo (0 ~ 0.76) prepared at different reduction temperatures: (a) Reduced at 550 ^oC; (b) Reduced at 600 ^oC. (◆) Mo_2C; (o) Ni; (*) $Ni_6Mo_6C_2$.

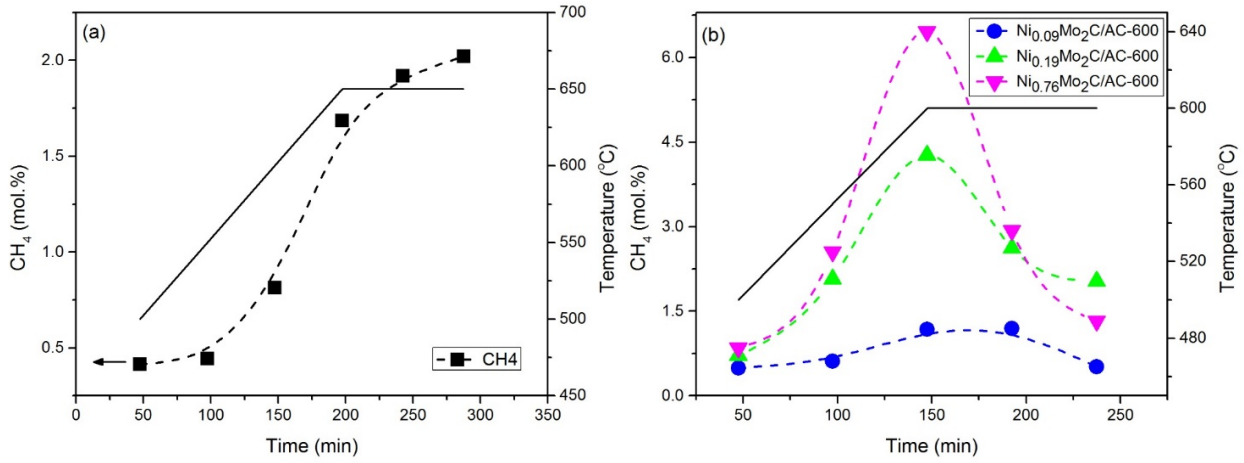

Figure 2: Profile of detected CH_4 (mol%) during carbothermal hydrogen reduction of the catalysts: (a) Mo_2C/AC-650 (■); (b) Ni-Mo_2C/AC with different ratios of Ni:Mo ((●) $Ni_{0.09}Mo_2C$/AC-600; (▲) $Ni_{0.19}Mo_2C$/AC-600; (▼)$Ni_{0.76}Mo_2C$/AC-600).

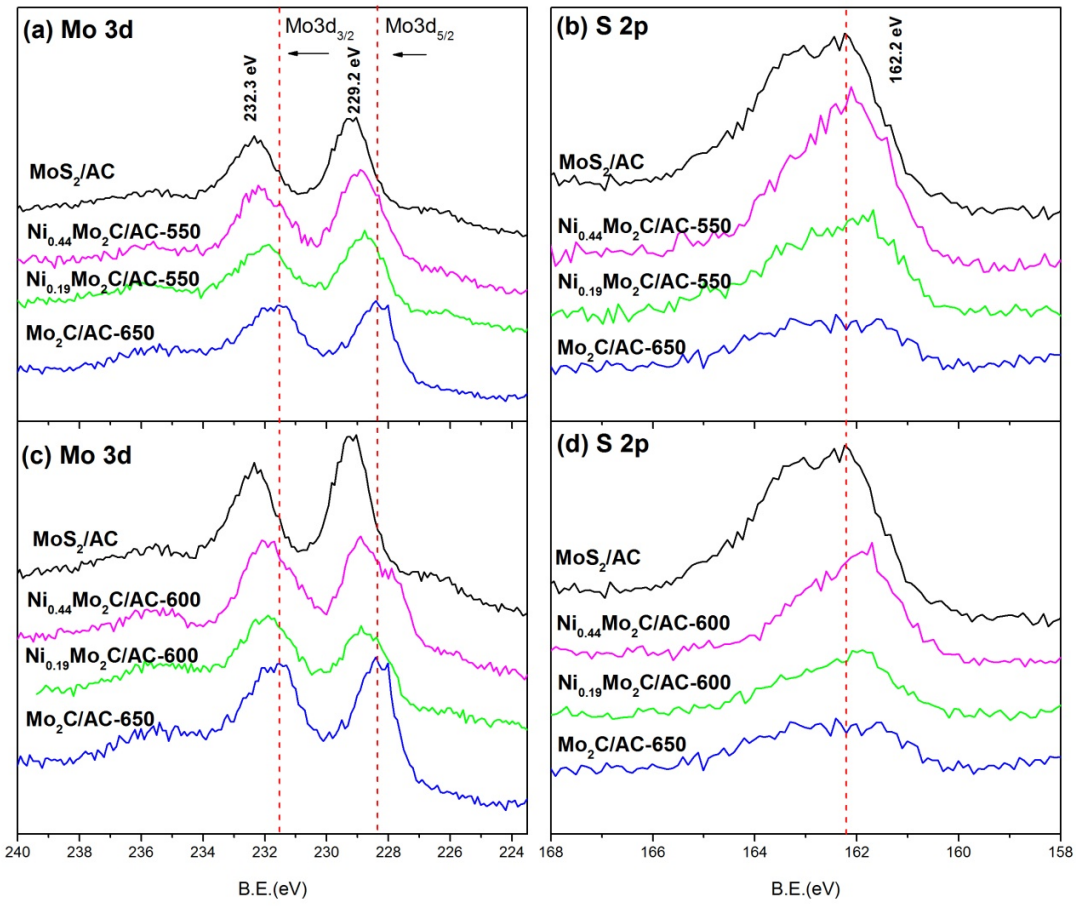

Figure 3: XPS narrow scan spectra of used MoS_2/AC, Mo_2C/AC and Ni_xMo_2C/AC-y catalysts. (a, c) Mo 3d; (b, d) S 2p. (The dashed lines in (a, c) indicate the position of Mo^{2+} species from Mo_2C; the dashed lines in (b, d) indicate the position of S^{2-} species from MoS_2.)

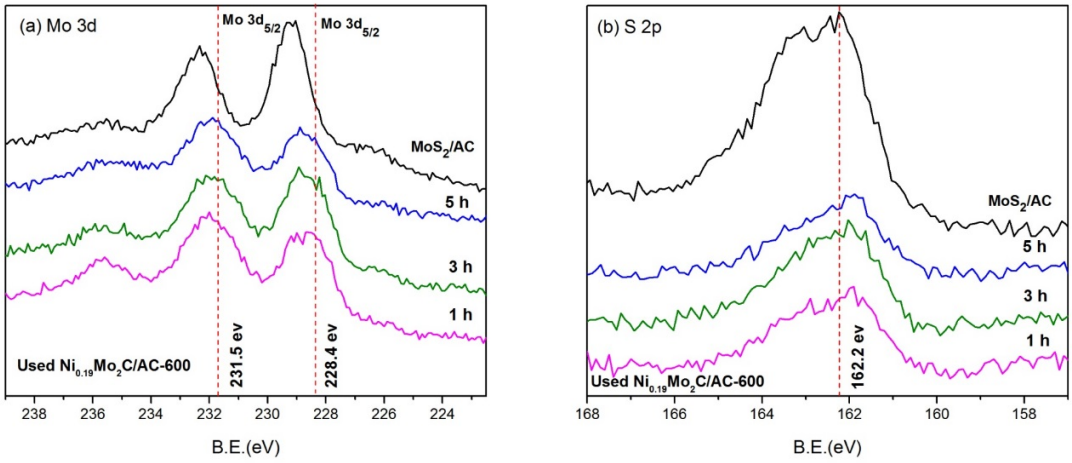

Figure 4: XPS narrow scan spectra of used $Ni_{0.19}Mo_2C$/AC-550 catalyst after HDS reaction for different periods. (a) Mo 3d; (b) S 2p.

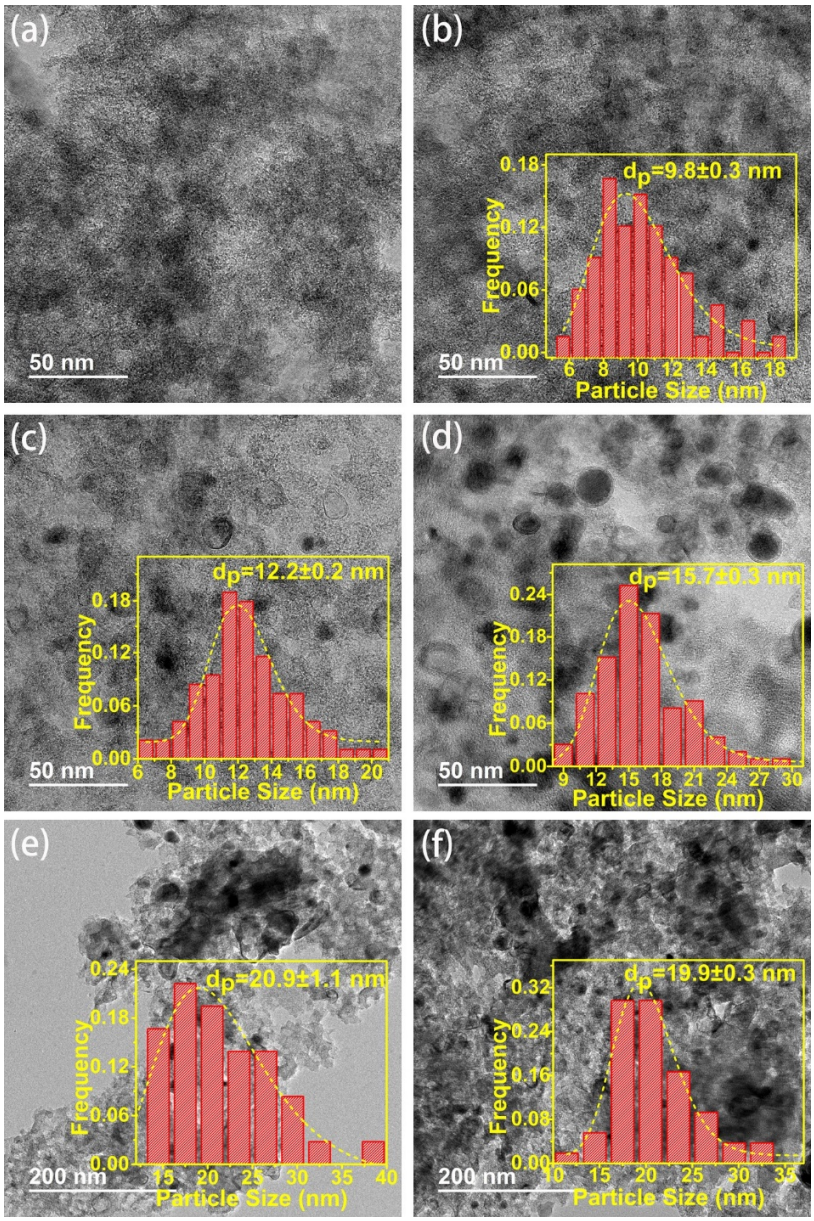

Figure 5: TEM images and cluster size distribution of used Ni-Mo_2C/AC catalysts with different Ni contents. (a) $Ni_{0.02}Mo_2C$/AC-600; (b) $Ni_{0.09}Mo_2C$/AC-600; (c) $Ni_{0.19}Mo_2C$/AC-600; (d) $Ni_{0.38}Mo_2C$/AC-600; (e) $Ni_{0.44}Mo_2C$/AC-600; (f) $Ni_{0.76}Mo_2C$/AC-600.

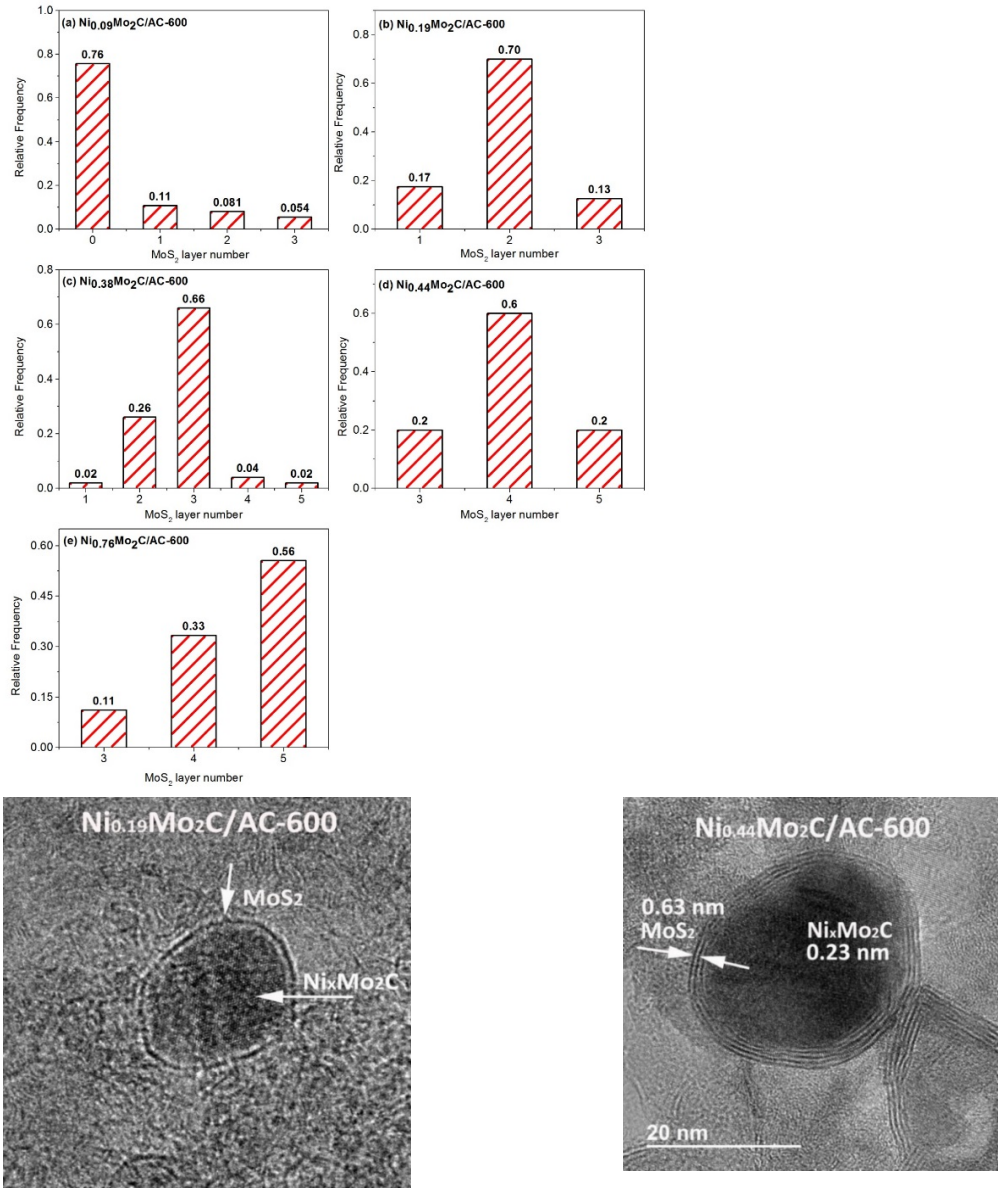

Figure 6: Distribution of MoS_2 layer numbers for used catalysts. (a) $Ni_{0.09}Mo_2C$/AC-600; (b) $Ni_{0.19}Mo_2C$/AC-600; (c) $Ni_{0.38}Mo_2C$/AC-600; (d) $Ni_{0.44}Mo_2C$/AC-600; (e) $Ni_{0.76}Mo_2C$/AC-600; Below there are two graphs of $Ni_{0.19}Mo_2C$/AC-600 and $Ni_{0.44}Mo_2C$/AC-600 used catalysts, respectively.

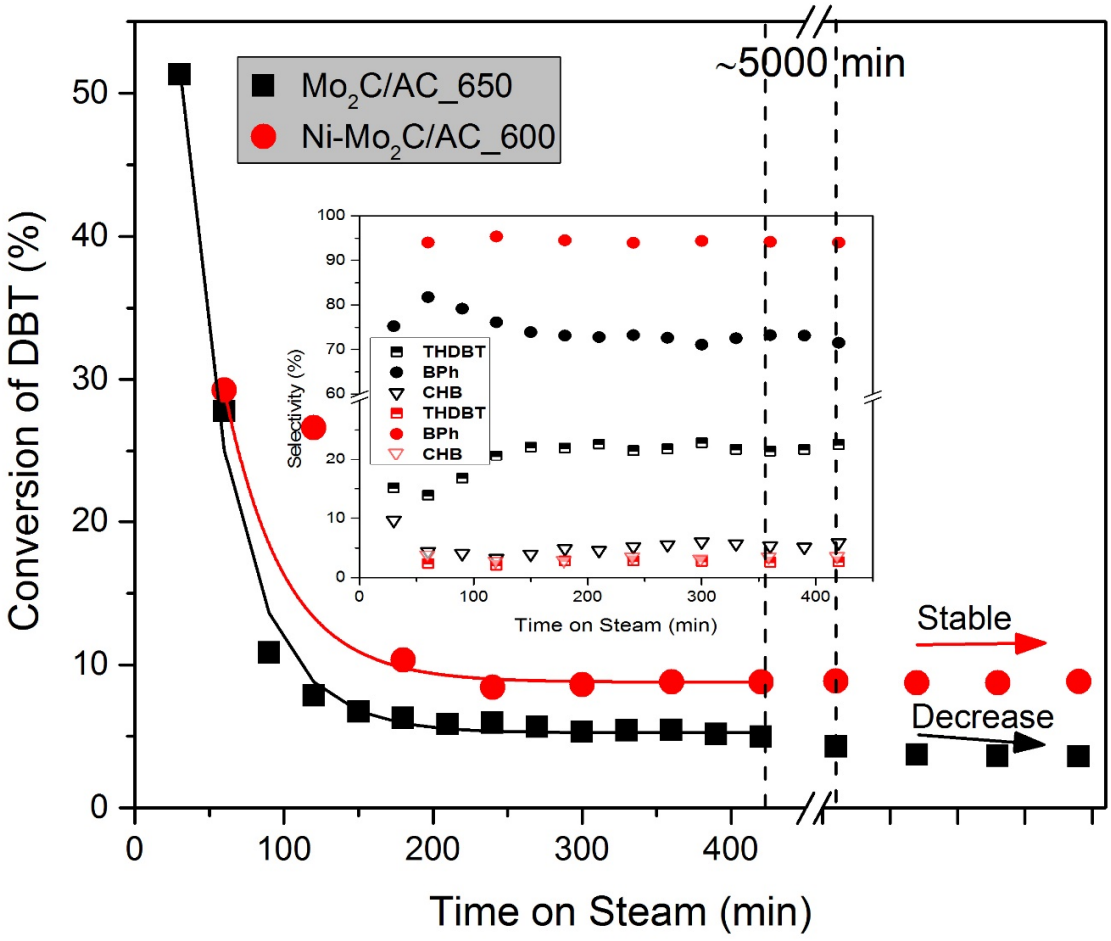

Figure 7: DBT conversion and product selectivity versus time on steam for $Ni_{0.19}Mo_2C$/AC-600 and Mo_2C/AC-650 catalyst, measured in the downflow fixed-bed reactor is at 310 °C, 4.1 MPa, H_2/feed volumetric ratio = 600 and LHSV = 8 h^{-1}

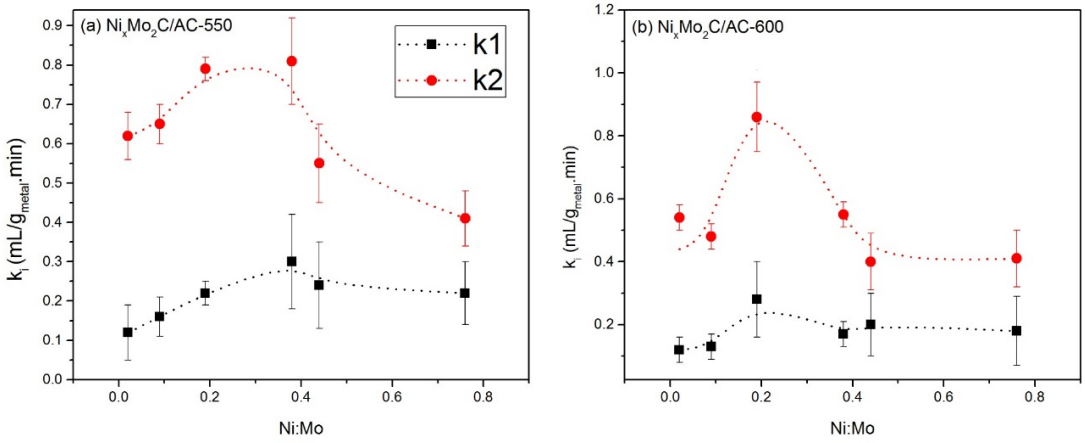

Figure 8: Kinetic parameters k_1, k_2 vs. Ni:Mo ratio of Ni-Mo_2C/AC catalysts: (a) reduced at 550 ^oC; (b) reduced at 600 ^oC. (…Trend line)

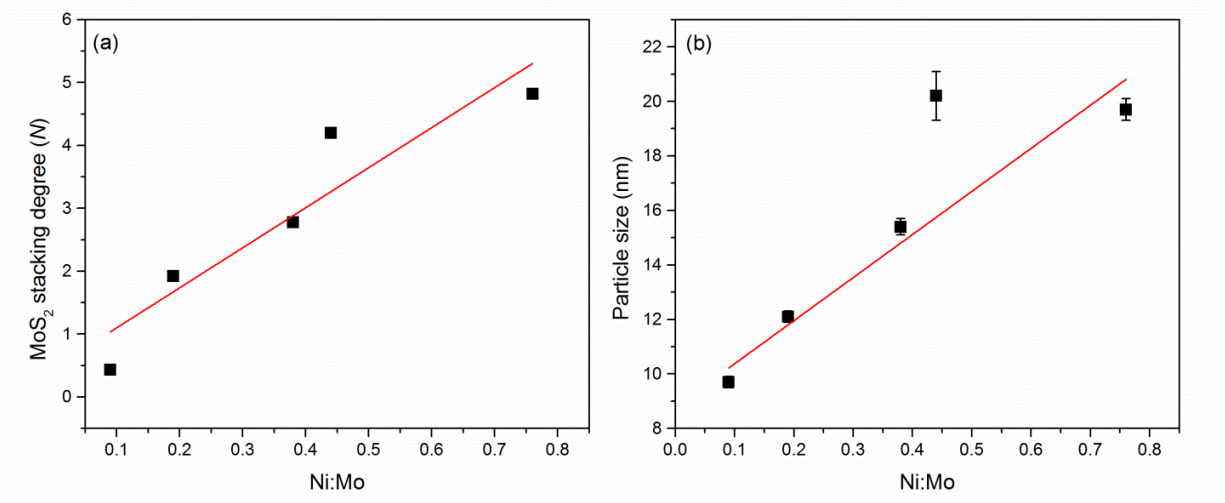

Figure 9: The correlation of Ni:Mo ratio to MoS_2 stacking degree (N) (a) and the average particle size (b). ―is the fitted line.

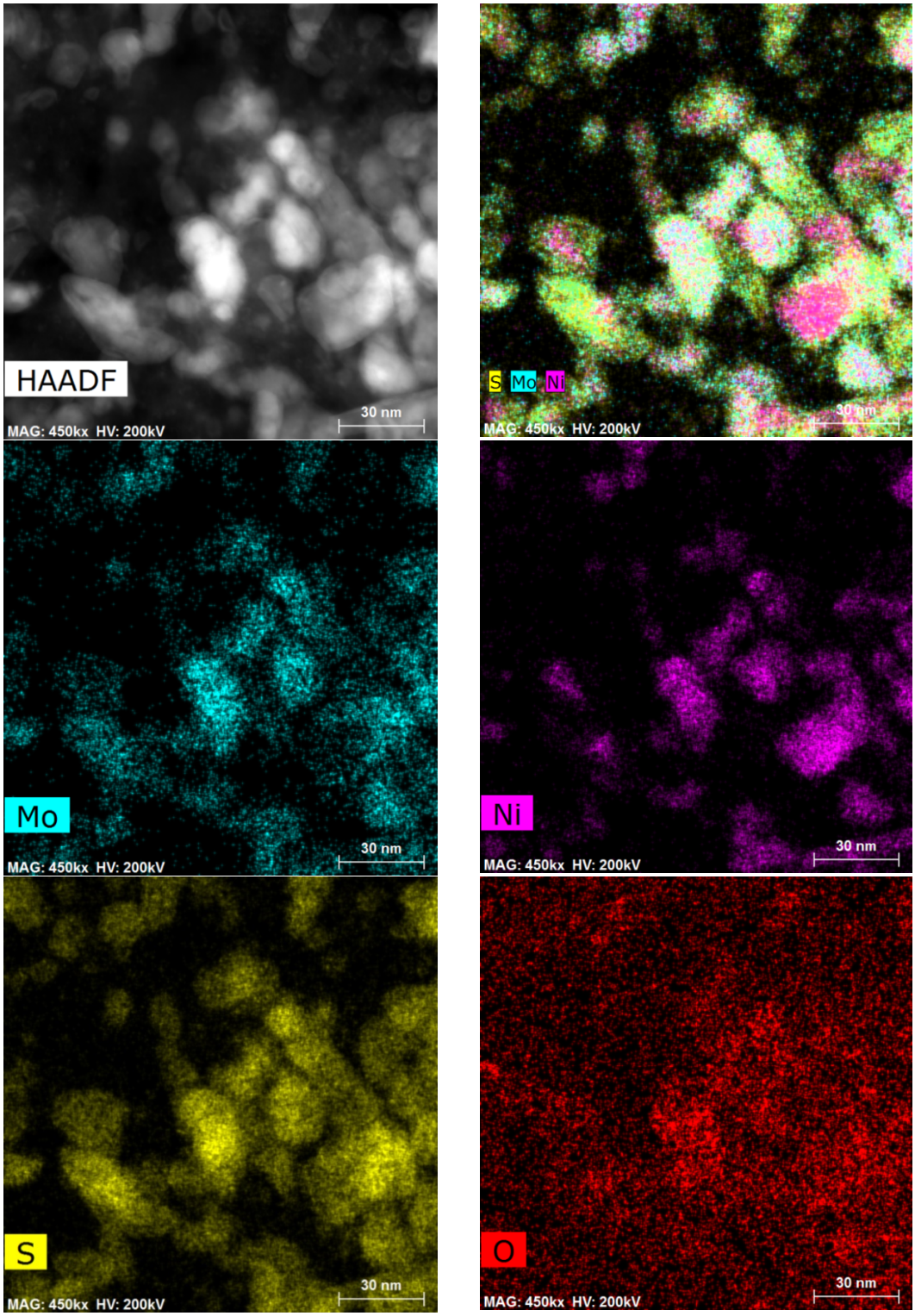

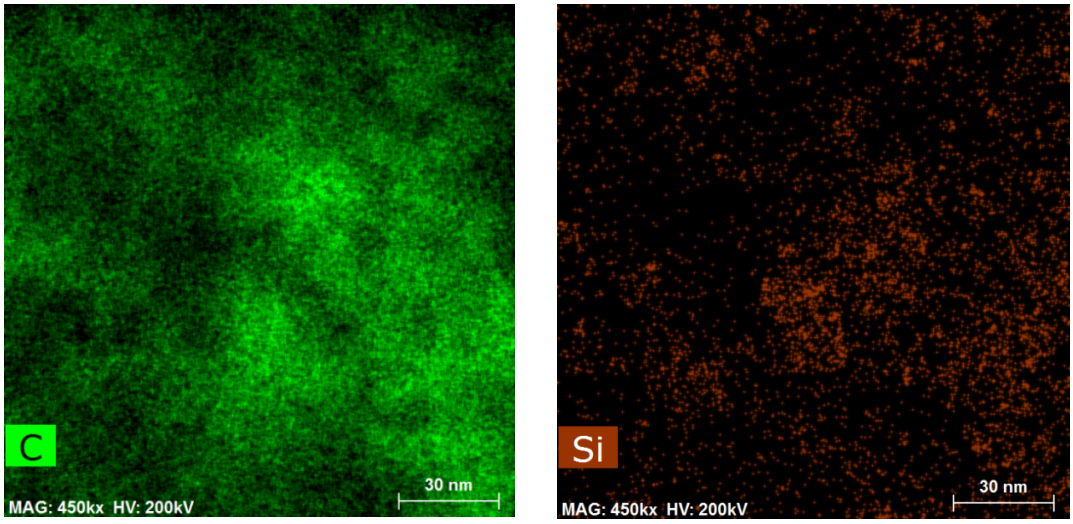

Figure 10: High angle annular dark field scanning (HAADF-STEM) image and energy-dispersive X-ray (EDX) elemental mapping of used $Ni_{0.19}Mo_2C$/AC-600 catalyst for elements Mo, Ni, S, O, C, and Si.

Table 1. XRD analysis of Ni_xMo_2C-600 catalysts and Mo_2C/AC-750 catalyst.

Catalyst	Phases	Diffraction peaks, 2θ			Lattice parameters (Å)	
		Mo_2C			a/b	c
		100	200	101		
10%Mo_2C/AC-750	β-Mo_2C	40.23	44.30	46.14	3.0050	4.7633
$Ni_{0.09}Mo_2C$/AC-600	β-Mo_2C	40.25	44.23	46.18	3.0032	4.7563
$Ni_{0.19}Mo_2C$/AC-600	β-Mo_2C	40.30	44.41	46.26	3.0000	4.7402

Table 2. Catalyst composition of fresh Mo_2C/AC-650 and Ni-Mo_2C/AC catalysts.

Ni:Mo[a]	Metal content (wt%)				Burn off % [b]	
	550 °C		600 °C		550 °C	600 °C
	Ni	Mo	Ni	Mo		
0.02	0.12	8.60	0.13	9.41	5	14
0.09	0.49	8.49	0.53	9.26	9	17
0.19	1.01	8.52	1.22	10.35	18	33
0.38	2.06	8.90	2.43	10.52	19	34
0.44	2.90	10.77	3.89	14.43	25	47
0.76	4.78	10.26	6.26	13.44	28	48

[a.] This is measured by ICP-OES

[b.] Burn off (%) is calculated by the mass difference before and after CHR divided by the mass before CHR, error ± 2%.

Table 3. Physical properties of fresh and used Ni-Mo_2C/AC catalysts prepared at reduction temperatures of 550 °C and 600 °C.

Ni:Mo	Surface area (m^2/g)				Pore size (nm)				V_{meso}/V_{total} (%)			
	Fresh 550	Used 550	Fresh 600	Used 600	Fresh 550	Used 550	Fresh 600	Used 600	Fresh 550	Used 550	Fresh 600	Used 600
0.00[a]	911	467	911	467	3.70	4.70	3.70	4.70	83	93	83	93
0.02	778	406	887	450	3.58	4.90	3.75	4.90	76	95	80	94
0.09	815	436	774	472	3.67	4.90	4.46	5.50	81	95	85	98

0.19	721	403	701	409	3.88	5.10	5.10	7.10	83	97	90	100
0.38	763	446	650	380	3.86	5.40	6.12	7.50	84	95	93	100
0.44	774	349	647	369	4.50	5.60	6.30	9.00	88	97	95	100
0.76	806	385	525	206	4.70	6.20	6.87	9.40	89	100	98	100

[a.] This is the unpromoted Mo_2C/AC-650.

Table 4. XPS and CHNS analysis of used (Ni)-Mo_2C/AC catalysts with different Ni:Mo ratios and different reduction temperatures.

Used catalyst[a]	**S, At%[b]**	**Mo, At%[b]**	**O, At%[b]**	**C, At%[b]**	**S/Mo atomic ratio, %**	**S[d], wt%**	**S[e], wt%**
10%Mo_2C/AC-650	0.43[c]	0.82	4.43	94.32	0.53	1.07	2.00
$Ni_{0.19}Mo_2C$/AC-550	0.90	0.64	3.68	94.78	1.41	2.23	3.24
$Ni_{0.44}Mo_2C$/AC-550	1.10	0.52	5.06	93.32	2.12	2.75	3.84
$Ni_{0.19}Mo_2C$/AC-600	0.67	0.68	4.99	93.67	0.99	1.65	2.22
$Ni_{0.44}Mo_2C$/AC-600	0.97	0.76	4.40	93.87	1.28	2.39	2.85

[a.] All of these used catalysts listed were recovered following 5 h HDS of DBT in the batch reactor;

[b.] These values are normalized;

[c.] Measured by XPS;

[d.] Surface adsorbed S wt% calculated based on XPS;

[e.] Bulk phase S wt% calculated based on CHNS analyzer.

Table 5. XPS and CHNS analysis of used catalysts (Mo_2C/AC-650 and $Ni_{0.19}Mo_2C$/AC-600) after HDS reaction in the batch reactor for different periods.

Used catalyst	**Reaction time (h)**	**S, At%[a]**	**Mo, At%[a]**	**O, At%[a]**	**C, At%**	**S/Mo atomic ratio, %**	**S[b], wt%**	**S[c], wt%**
10%Mo_2C/AC-650	1	0.20[d]	0.68	3.73	95.39	0.30	0.51	1.33
	3	0.30	0.70	4.08	94.92	0.43	0.75	1.47
	5	0.40	0.69	4.44	94.47	0.59	1.01	2.00
$Ni_{0.19}Mo_2C$/AC-600	1	0.47	0.68	4.01	94.83	0.69	1.18	1.40
	3	0.58	0.68	3.41	95.33	0.87	1.46	1.83
	5	0.67	0.68	4.99	93.67	0.99	1.65	2.22

[a.] These values are normalized;

[b.] Surface absorbed S wt% calculated based on XPS;

[c.] Bulk phase S wt% calculated based on CHNS analyzed;

[d.] Measured by XPS.

Table 6. Normalized intensity of selected ions (containing the most abundant isotope ^{32}S) calculated based on TOF-SIMS spectra of used catalysts of 10%Mo_2C/AC-650 and $Ni_{0.19}Mo_2C$/AC-600.

Calculated parameters	**Used catalyst**	
	10%Mo_2C/AC-650	**$Ni_{0.19}Mo_2C$/AC-550**
RI (S)[b] (x 10^{-2})	1.91 ±0.12 [a]	2.27±0.10
RI (MoO_xS_y)[c] (x 10^{-2})	0.13±0.01	0.25±0.01
RI (MoO_xS_y)/RI (S) (%)	6.81±0.68	11.01±0.66
Distribution of Identified MoO_xS_y species (RI') [d] (%)		
RI'(MoS) [e]	13.09±0.87	6.98±0.16
RI'(MoOS) [f]	52.30±0.46	56.07±0.43
RI'(MoO_2S or MoS_2) [f]	24.28±0.45	26.46±0.39
RI'(MoO_3S or $MoOS_2$) [f]	6.60±0.40	4.45±0.05
RI'(MoO_2S_2 or MoS_3) [f]	3.72±0.28	6.05±0.17

[a.] Estimated as standard deviation.

[b.] The relative intensity (RI) of total identified S to total ions: $RI(S)= \Sigma S^-/\Sigma I^+$;

[c.] The relative intensity (RI) of total identified $MoO_xS_y^-$ to total ions: $RI=\Sigma MoO_xS_y^-/\Sigma I^+$;

[d.] This distribution is based on all the identified $MoO_xS_y^-$ species;

[e.] Prime relative intensity (RI') of MoS ions to total MoO_xSy ions: $RI'= MoS/\Sigma MoO_xS_y^-$

[f.] All of these is similar to e's calculation by changing numerator.

Table 7. Kinetic model parameters estimated for the HDS of DBT after the 1st hour of the reaction in the batch reactor over Ni-Mo_2C catalysts at 623 K and initial P_{H_2}=2.1 MPa.

Ni_xMo_2C/AC-550	Kinetic Parameter (mL /g_{metal}.min)					Ni_xMo_2C/AC-600	Kinetic Parameter (mL /g_{metal}.min)				
	k_1	k_2	k_3	k_{total} (k_1+k_2)	$S_{DDS/HYD}$ (k_2/k_1)		k_1	k_2	k_3	k_{total} (k_1+k_2)	$S_{DDS/HYD}$ (k_2/k_1)
0.02	0.12±0.07[a]	0.62±0.06	2.21±1.48	0.74±0.13	5.00±2.87	0.02	0.12±0.04	0.54±0.04	1.99±1.32	0.67±0.08	4.40±1.59
0.09	0.16±0.05	0.65±0.05	1.78±1.05	0.81±0.10	4.20±1.48	0.09	0.13±0.04	0.48±0.04	1.89±1.11	0.61±0.08	3.55±1.12
0.19	0.22±0.03	0.79±0.03	4.75±1.13	1.01±0.05	3.58±0.47	0.19	0.28±0.12	0.86±0.11	7.77±7.83	1.14±0.22	3.06±1.33
0.38	0.30±0.12	0.81±0.11	4.84±3.79	1.11±0.23	2.71±1.18	0.38	0.17±0.04	0.55±0.04	4.95±2.81	0.72±0.08	3.22±0.88
0.44	0.24±0.11	0.55±0.10	4.12±3.86	0.79±0.21	2.25±1.10	0.44	0.20±0.10	0.40±0.09	6.25±6.76	0.60±0.19	2.06±1.19
0.76	0.22±0.08	0.41±0.07	3.41±2.80	0.63±0.15	1.89±0.78	0.76	0.18±0.11	0.41±0.09	4.71±6.01	0.59±0.20	2.36±1.54

[a.] estimated standard deviation.